Efficient Processing of Distributed Acoustic Sensing Data Using a Deep Learning Approach

Lihi Shiloh, Avishay Eyal, *Senior Member, IEEE*, and Raja Giryes, *Member, IEEE*

***Abstract*—Automatic processing of fiber-optic distributed acoustic sensing (DAS) data is highly desired in many applications. In particular, efficient algorithms for detection of events of interest and their classification are of the utmost importance. Classical machine learning algorithms are problematic as they require handcrafted features to be extracted and their adaptation to other sites or other DAS systems is difficult. In contrast, artificial neural networks (ANN) learn by themselves how to extract relevant features and signatures in the training phase. The training phase, however, necessitates the generation of a large database of tagged events (train-set). In this paper, we describe a new method for generating train-sets for DAS ANNs and its experimental testing. The method is based on the generative adversarial net (GAN) methodology. The use of a GAN facilitated an efficient generation of train-sets from a computer simulation of the DAS system. The train-set was then used to train an ANN, which processed experimental data from 5- and 20-km sensing fibers. Significant improvement in performance was obtained with respect to ANN trained by only simulation data or experimental data.**

***Index Terms*—Optical fiber sensors, distributed acoustic sensing, machine learning, neural networks, seismic measurements.**

I. Introduction

With the significant progress in fiber optic Distributed Acoustic Sensing (DAS) in recent years [1]–[3], efficient automatic processing schemes of its raw data have become highly desired. DAS systems are capable of continuously monitoring acoustic signals and vibrations along tens of kilometers with high sensitivity and high update rate. This is accomplished using a conventional telecom-type optical fiber whose Rayleigh backscatter profile is measured repeatedly by a reflectometric method. DAS technology has many advantages over competing technologies as it is simple to deploy, immune to electromagnetic interference, cost-effective and requires no inline amplification or power supply. Whether it is based on Optical Time Domain Reflectometry (OTDR) or Optical Frequency Domain Reflectometry (OFDR), a DAS system comprises an interrogator and a sensing optical cable. The backscattered light is detected and the output of the detector is processed to yield spatially encoded acoustic and vibration signals. With meter scale spatial resolution and tens of kilometers sensing range, DAS is ideal for applications such as border protection, intrusion detection, railway monitoring, pipeline security and many other potential applications. A DAS system typically acquires ∼1000 complex backscatter profiles per second and processes them in real time. The data rates of optical data generally exceed 10 Mbyte/s, and may accumulate to more than 1 Tbyte of data per day. In order for this huge amount of data to be useful, it is imperative to develop automatic, efficient and accurate tools for processing the recorded signal. Specifically, detection, classification and localization of recorded events is of the utmost importance.

Due to the complexity of the optical data, its high bitrate and the need for real time processing, state-of-the-art machine learning algorithms are ideal candidates to extract the desired information. Classical machine learning algorithms require handcrafted features to be extracted from the data in order to train and predict. Several studies have been published using such techniques [4]–[6].

More recently, Artificial Neural Networks (ANN), which learn by themselves how to extract relevant features and signatures in the training phase, have been employed for DAS data. The power of ANN technology cannot be overstated and its range of applications have been increasing tremendously in recent years [7]–[9]. What started as a tool for computer vision and image processing [10], has expanded to many other fields such as medicine [11], audio processing [12] as well as optics. In the optics field it was used for end-to-end modeling of a complete optical communications system [13], for applications of computational imaging [14], [15], for controlling self-tuning mode-locked lasers [16], for improving optical microscopy [17] and more. Despite their growing popularity, only few studies investigated ANNs for DAS applications [18]–[20]. For example, Liehr *et al.* [21] utilize ANN to predict strain in real-time applications using the wavelength-scan coherent optical time domain reflectometry approach. Their method allows improvement in strain noise and linearity of the sensor response. Aktas *et al.* [22] used a 5 layer Convolutional Neural Network (CNN) to classify 6 seismic events at a vicinity of the sensing fiber. Tejedor *et al.* [23]–[26] developed a complex system composed of a Gaussian Mixture Model (GMM) along with Multilayer Perceptron (MLP) to extract features and classify 8 seismic events. The two latter studies have shown good classification results on long DAS systems (>20 km). It is well known that the effectiveness of these advanced tools depends strongly on the training phase.

Manuscript received January 12, 2019; revised May 23, 2019; accepted May 26, 2019. Date of publication May 29, 2019; date of current version September 18, 2019. This work was supported in part by the ERC-StG Grant 757497 (SPADE), in part by the Shlomo Shmeltzer Institute for Smart Transportation, and in part by the NVIDIA under the GPU grant. *(Corresponding author: Lihi Shiloh.)*

The authors are with the Faculty of Electrical Engineering, Tel-Aviv University, Tel Aviv 6997801, Israel (e-mail: lihishiloh@mail.tau.ac.il; avishay1@tauex.tau.ac.il; raja@tauex.tau.ac.il).

Color versions of one or more of the figures in this paper are available online at http://ieeexplore.ieee.org.

Digital Object Identifier 10.1109/JLT.2019.2919713

The training phase, in turn, necessitates generation of a large database of tagged events. In the case of DAS, generation of such a database, even with human tagging, is particularly difficult and, as appears in the aforementioned research reports, requires significant resources of time and labor. The requirement for large amounts of training data is one of the disadvantages of using ANNs. Another great disadvantage of all the above-mentioned techniques is that their adaptation to other sites or other DAS systems is likely to require significant time and human resources as some characteristics and features of the processed data may vary. This is especially true for ANNs that heavily rely on particular characteristics of the training data.

An approach to deal with these disadvantages is via computer simulations. Indeed, this may significantly simplify the ANN development stage and allow tremendous saving in time and costs. However, this approach requires highly accurate modeling of the optical DAS system, the generation and propagation of the seismic/acoustic waves in the medium and the interaction between the waves and the fiber. The physical parameters and details needed for such modeling are rarely available.

Recently we proposed a solution to this problem [27]. Using a Generative Adversarial Network (GAN [28]) we efficiently increased the training dataset with simulation signals [27], [29]. A GAN is a tool for learning the distribution of a given data. It is composed of two models, a generator and a discriminator, trained as adversaries. The generator is trained to capture the data distribution, while the discriminator is trained to differentiate between generated data and real data. The training is terminated when the generator generates data which the discriminator fails to discriminate from the real data. The GAN architecture is finding more and more applications since its introduction in 2014. It was proved successful in rendering of image scenes [30], inpainting [31], 3D modeling [32] and more. In the current study, it is shown that this technique is also useful in refining synthetic DAS data of 5 km and 20 km long sensing fibers and enabling them to mimic real experimental data. The synthetic data was generated via finite element simulations. To increase the validity and diversity of the training set, the simulations included the effect of noise on the optical measurement system and other parameters such as speed and attenuation of the seismic waves or the distance of the excitation from the fiber. Detailed description of the simulation is given in Section IV.B. This simulation data was refined using the trained generator model so that they will represent the true experimental data more faithfully when training the final classification network. We fine-tuned this network by using an additional small set of tagged experimental data.

In the current paper the preliminary results presented in [27] are expanded. The simulations at the basis of the method and the configurations of the deep-learning networks are described in detail. Multi-class classification performance on the previous 5 km sensing fiber and new results from a 20 km fiber is presented. In these in-campus experiments, human footsteps and vehicles at the vicinity of the fiber were detected from ambient noise and classified using the proposed approach.

In the realistic case of a long sensing fiber with diverse ambient noise, different versions of FiberNet, appropriately trained, can be used to process different sections of the fiber.

The paper is organized as follows: Section II presents the methods used to apply deep learning for processing of DAS data with emphasis on the GAN approach. Sections III and IV, respectively, detail the networks architecture and the data sets used. Section V presents classification results and Section VI concludes.

II. Methods

In this study, an OFDR system is used to interrogate the sensing fiber. Detailed description of the principles of OFDR-based DAS can be found in [33]. Briefly, in OFDR the laser instantaneous frequency is scanned linearly with time. The light is split to reference and interrogation beams. The interrogation beam is launched into the sensing fiber. The backscatter from the fiber is mixed with the reference and the result is detected by a balanced detector. Each position in the fiber yields a different beat frequency at the detector output. Fourier transform of the detector output yields the complex backscatter profile of the fiber. As in many other DAS systems, OFDR gives both the amplitude and phase of the backscatter signal. Both these signals can be used as inputs to the detection and classification signal processing layer and both have their respective advantages and disadvantages. The use of the amplitude is simple and robust. The use of phase, on the other hand, requires more elaborate processing, but can provide linearity of the signal with respect to the excitation and enhanced SNR [34], [35]. A disadvantage of phase processing is the risk for phase wrapping and phase ambiguity when the excitation is strong. Our use of ANN for the processing of the raw data enabled a straightforward fusion of both modalities.

The complex fiber profile, acquired by the DAS system, was parsed to segments. In this study all processing was performed on segments, which were taken from a buried section of the fiber. In realistic scenarios all fiber sections can be processed independently in parallel to obtain real-time operation.

In each segment, both the amplitude and the phase difference between consecutive sample resolution cells (*differential phase*) were calculated. These two images (amplitude and differential phase) were normalized independently and appended to create a 'two channel image' (similarly to RGB images but with two channels instead of three). The two-channel image, corresponding to 0.5 s time interval and specified fiber segment, is the input to the network. With update rates of 2000 scans/s and 1000 scans/s and fiber segments of $\sim$90 and $\sim$120 m for the 5 km and 20 km experiments respectively, the corresponding input image sizes were 50×500 and 32×250 pixels, respectively.

Having short time intervals reduced the processing latency and made the method compatible with real-time operation. It enabled capturing fast occurring details of the seismic excitations but led to a presence of one or zero human steps in each image. This means that the tested network did not enjoy longer time-scale-features, primarily cadence rate. An additional classification layer, which uses this information, may significantly

improve the performance. In addition, the segment size used determined the localization abilities of the system, since the position of the classified target is within the known segment.

One of the problems with training neural networks for DAS data is the data acquisition and tagging. To overcome this issue, we trained the networks on simulated data. As there is typically considerable difference between simulated data and the true data, we used a neural network that adjusted the simulated data such that they became more similar to the true data. As mentioned above, for this purpose we used GANs.

The GAN architecture used in this study is called Conditional GAN (C-GAN [23]). This version of GAN connects the generator and discriminator through some extra information in a conditional manner. In this case, the generator learns to generate from a fake sample with a specific condition rather than a generic sample from unknown noise distribution.

A specific C-GAN variant combines simulation and experimental data [29] and is referred to as SimGAN. In the SimGAN methodology, the generator is trained to transform simulation data to appear realistic, while the discriminator is trained to differentiate between generated data and real data. It is very useful for applications that suffer from an insufficient number of training examples that cannot be artificially increased using simulations (due to modeling complexity). It enables the increase of the size of the database for further analysis. For example, eye gaze estimation, 3D objects rendering and face rotation, have limited databases that restrict their classification performance. Using this methodology, their classification performance has increased [29]. As mentioned above, experimental data in the DAS case is difficult to acquire and/or simulate. Therefore, the SimGAN methodology can be used to refine relatively simplified simulations to have the features of real field experiment data. This can increase the efficiency of the training phase of a classification ANN.

Denote the generator, G_θ, and the discriminator, D_ϕ, where θ and ϕ are their weights, respectively, the real experimental data as $y \in \mathcal{Y}$, and the simulation data as $x \in \mathcal{X}$. The cross-entropy loss used to optimize the discriminator is formulated as follows:

$$\mathcal{L}_D(\phi) = -\sum_i \log\left(D_\phi\left(G_\theta\left(x_i\right)\right)\right) - \sum_j \log\left(1 - D_\phi\left(y_j\right)\right). \tag{1}$$

The generator is trained to accurately mimic genuine data using two weighted loss functions:

$$\mathcal{L}_G(\theta) = -\sum_i \log\left(1 - D_\phi\left(G_\theta\left(x_i\right)\right)\right) + \lambda \left\| G_\theta\left(x_i\right) - x_i \right\|_1. \tag{2}$$

The first term is the cross-entropy term that aims at "fooling" the discriminator, i.e., making the generated data looks like the experimental one. The second term is a regularization term weighted by a scalar λ that does not allow the generated data deviate much from the input simulated data. The purpose of this term is to keep the class information in the generated sample, i.e., if the input corresponds to a step, we want the generated realistic sample to contain a step as otherwise we will not be able to use the same labels of the simulated data. We used the L_1 norm, to allow robustness in the deviation from the input as is common in image rendering.

TABLE I
FIBERNET ARCHITECTURE

Layer	Size in	Size out
Conv2D	5km: 500x50x2 20km: 250x32x2	5km: 500x50x3 20km: 250x32x3
VGG16 (13 conv. layers with max pooling)	5km: 500x50x3 20km: 250x32x3	5km: 15x1x512 20km: 7x1x512
FC1 (ReLU+BN)	5km: 15x7680 20km: 7x3584	1x4096
FC2 (ReLU+BN)	1x4096	1x4096
FC3 (ReLU+BN)	1x4096	1x128
Logits (softmax)	1x128	1xN_{classes}

After converging to an optimal generator, the classification network is initially trained using the refined simulation data. The next phase is fine-tuning the network using a smaller experimental data-set. The purpose of this second training stage is to fine-tune the network to a more optimal working point with respect to the system's data.

The technique was implemented using Keras backend (TensorFlow version 1.8) with i7 CPU, 32 GB RAM and an NVIDIA GeForce GTX 1080 Ti GPU (11 GB).

III. NETWORK ARCHITECTURE

Since the task of classifying seismic events, from the input described above, is analogous to classification of objects from images, the ANN model we employed was a Convolutional Neural Network (CNN), which is commonly used for classification, segmentation and image denoising [7]–[9]. The architecture was based on Oxford's VGG16 [8], which is known for its success in classifying the ImageNet dataset [37]. We added a convolutional layer at the network's input to match the original number of channels in VGG (with a kernel size of 5, a unit stride and ReLU as the activation function), and also a fully-connected layer at the end (with ReLU as the activation function and batch normalization for regularization). The VGG16 convolution layers' weights were initialized by the ImageNet pre-trained values, and the other layers were initialized with random weights. All layers were trained. The input images' channels were normalized, independently, to the range $[-0.5, 0.5]$. See Table I for the full architecture of what we refer to as FiberNet.

The 5 km architecture required 127 M FLOPs and the 20 km architecture 93 M FLOPs. The reason for the difference lies in the fact that the input sizes were different, i.e., 50×500 and 32×250 for the 5 km and the 20 km respectively. Note though that it is possible to independently process each segment, which allows a parallel processing of the whole fiber. To check the feasibility of the parallel computing approach the following tests were made: the 20 km fiber was parsed to 167 non-overlapping segments and the 5 km fiber was similarly parsed to 56 segments. In each case all the segments were processed in parallel by the GPU. These parallel calculations took roughly $\sim$100 ms in both cases. Considering that each segment corresponded to a duration

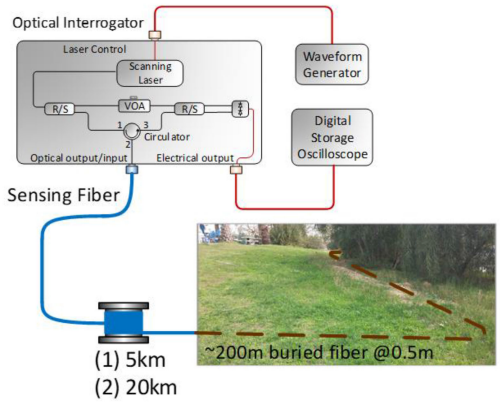

Fig. 1. Optical setup.

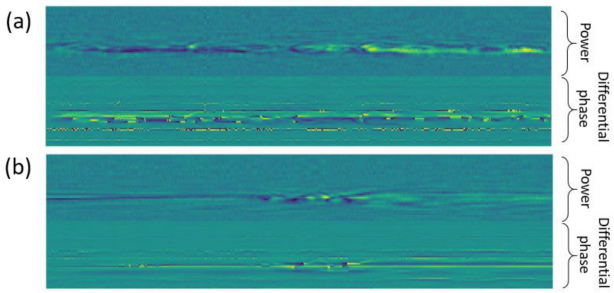

Fig. 2. Experimental examples of 5 km sensing fiber: (a) vehicle (b) footstep.

of 0.5 sec, the method is potentially compatible with real-time operation.

The GAN's discriminator model has the FiberNet's architecture. To train a multi-class GAN, the final fully-connected layer is implemented with $1 + N_{\text{classes}}$ outputs to differentiate between: noise, footstep, vehicles and simulations [38], [39]. The generator consists of a 6-layer residual network, inspired by its performance in images denoising [40]. A 3×3 convolution kernel with 65 filters is used for each layer, where one of them is used to calculate the residual image. The weight λ from (2), is set to 10^{-5}. In each GAN training step, the generator is trained on 12 batches and the discriminator is trained on one batch. Each batch consists of 30 signals. An example of the refiner effect on a footstep simulation is shown in Fig. 4. In this figure (and also in Fig. 2 and Fig. 3), the two image channels are shown: the upper image is the power and the lower image is the differential phase. Fig. 4(a) demonstrates a footstep generated by simulation while Fig. 4(b) shows its refined version after propagation through the generator. Notice the change in the signature and background noise.

Training the FiberNet classification network consisted of two phases: first using refined simulation data and then fine-tuning with experimental data. Training used a batch-size 30, and data augmentation for more robust performance. The augmentation included flipping the image along the fiber distance axis and randomly translating it on both axes. Optimization was performed using Stochastic Gradient Descent (SGD).

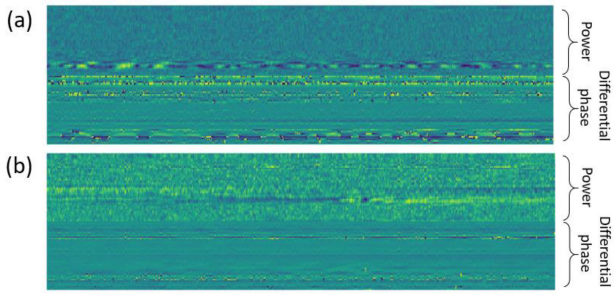

Fig. 3. Experimental examples of 20 km sensing fiber: (a) vehicle (b) footstep.

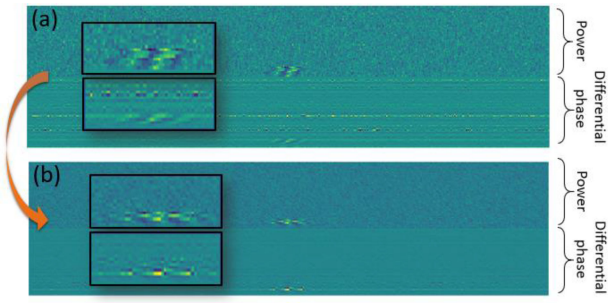

Fig. 4. Simultion of a seismic footstep signature from a 20 km DAS system (a) and its refined image (b). The insets zoom-in on the excitation signature to show fine details.

IV. Datasets

The datasets used in this study were of two types: datasets recorded in field experiments and datasets generated by computer simulations. Both datasets were used to train the GAN and the classification networks. The simulation datasets comprised ∼70 k images for the 5 km fiber and ∼150 k for the 20 km fiber. The experimental datasets comprised ∼49 k images taken with the 5 km sensing fiber and ∼10 k images with the 20 km fiber. The smaller number of signals in the 20 km case was a result of the very noisy measurement conditions in our (in-campus) test field. These conditions led to degraded SNR and limited time for recording. Hence, additional simulations were added to the training phase in this case.

The test sets were recorded on different days than the training datasets and were generated by different subjects. Specifically, the footsteps correspond to a ∼75 kg person in the test set and to a ∼60 kg person in the train set. The vehicle was a small campus car in the test set and Renault Kangoo in the train set. Test sets consisted of 135 images per class for the 5 km fiber and 224 images per class for the 20 km fiber.

The rest of this section describes in detail the generation of the experimental and simulation datasets.

A. Experiments

Field experiments were conducted at the backyard of Tel-Aviv university school of Electrical Engineering. 200 m of telecom-type optical cable were buried ∼0.5 m below the ground surface. The rest of the cable was deployed to the author's lab where additional fiber spools could be concatenated to it. Interrogation

was performed by a self-built OFDR DAS system, comprising an ultra-coherent laser with central wavelength of 1550.12 nm [2], [33]. Two sensing fibers were used in this study- one with a 5 km spooled fiber preceding the buried cable and the other with a 20 km spooled fiber (see Fig. 1). The sensing fiber scan rates were 2 kHz and 1 kHz for the 5 km and 20 km fibers respectively. In OFDR the processing window is the portion of the scan period, which is sampled and processed. The processing comprises primarily of a Fourier transform, which yields the full fiber complex reflection profile. In our experiments, the processing window was set to 13.1 μs, which determined the frequency range that is swept by the laser and hence determined the sampling and spatial resolution of the measurements. The optical sampling frequency was set to 1.25 Gsamples/s. The sampling resolution (after FFT) was $\sim$1.8 m/sample and $\sim$3.8 m/sample for the 5 km and 20 km experiments respectively. The spatial resolutions for each experiment was estimated, based on simulations, to be $\sim$5.5 m and $\sim$10.3 m respectively. In reality, these values were probably slightly bigger due to imperfections in the scan which were not taken into account by the simulation.

As mentioned above, the lengths of the fiber segments used as inputs to the ANNs corresponded to $\sim$90 m for the 5 km fiber and $\sim$120 m for the 20 km one. Examples of an input image for 5 km sensing fiber and 20 km sensing fiber are presented in Figs. 2 and 3 respectively.

In both figures, (a) corresponds to a recording of a vehicle at the vicinity of the fiber and (b) corresponds to a footstep. All excitations were performed at the vicinity of the buried fiber cable, i.e., 2–3 meters. The lower SNR in the case of the 20 km fiber is evident. Evaluation of the Power Spectral Densities (PSDs) of the differential phases, via averaging over all noise-tagged segments, yielded $30\ \mathrm{mrad}/\sqrt{\mathrm{Hz}}$ and $55\ \mathrm{mrad}/\sqrt{\mathrm{Hz}}$ for the 5 km fiber and 20 km fiber respectively. This distance-dependent noise is attributed mainly to random deviations from linearity of the laser frequency scan. A closely related effect is deterministic deviation from linearity [41]. This effect, which is also present in the current setup, led to a distance-dependent degradation in the spatial resolution, smearing of the signal and an additional deterioration in the SNR. Another noise source is the additive detection noise. It should be emphasized that non-ideal conditions such as these are actually desired in this work, which strives to prove the effectiveness of ANN for DAS in realistic conditions.

B. Simulations

To generate synthetic datasets of events of interest, a computer simulation was developed. The computer simulation had two main parts: an optical part and a seismic part. The optical part repeatedly produced a complex backscatter profile of a synthetic sensing fiber, similar to the description in [42]. After each cycle, the phases of the reflection coefficients were updated to simulate the externally induced acoustical perturbations (described below). To generate the complex backscatter profile, the fiber was represented by its impulse response. The impulse response was generated by dividing the fiber into small sections of length of 8 cm. For each section a backscatter coefficient was drawn from a complex normal distribution. The optical loss of the fiber (-0.2 dB/km) was taken into consideration by multiplying each coefficient with its appropriate loss term. The backscatter signal, at the input of the coherent receiver, was obtained by convolving the fiber's impulse response with the input waveform. Once the backscatter signal was known it was added to the reference (the input waveform). The square magnitude of the resulting signal was calculated to yield the detector output. Finally, Fourier transform of the detector output yielded the simulated complex backscatter profile of the fiber.

One of the major advantages of SimGAN [29] is that it saves the need to meticulously simulate a training dataset and allows using simpler models. It is particularly useful when there are important physical parameters which are unknown. The models are based on empirical observations and their usefulness is tested according to the performance of the network.

Two types of noise signals were introduced into the optical part: additive detection noise and phase noise. The additive detection noise, which represents shot noise and thermal noise, was added to the generated detector output. Laser phase noise was introduced by adding a noise term to the instantaneous frequency of the laser, which was based on a sinusoidal scan for a fast and accurate measurement [33]. The noise parameters were manually tuned to best fit the experiments. Despite this tuning procedure, uncertainties in the modeling of the noise and the values of its parameters led to apparent differences between the simulated and measured noise.

The seismic part of the simulation assumed wavelets emanated from a point source (described in the following paragraph) propagating radially in a homogenous medium at a speed of $\sim$200 m/sec, which corresponds to seismic surface waves.

Two excitations that were studied in this work, human footsteps and vehicles, were modelled. The temporal and spectral signatures of the seismic events were determined empirically by analyzing the experimental results. Since the physical models of seismic propagation and coupling to the fiber cable are very complex, the GAN architecture was employed to mitigate this gap. The excitations were introduced into the simulation as modifications to the phase response of the sensing fiber. The modifications were made in each scan period. Footsteps are modeled as wavelets with center frequencies uniformly distributed in the range 55–60 Hz and with duration uniformly distributed between 13.3 ms and 13.5 ms. Synthetic vehicles' signals were created by generating white Gaussian noise and filtering it to the range 150–270 Hz, according to the power spectral density of the experimental samples.

An example of a footstep simulation at the vicinity of 20 km fiber is presented in Fig. 4(a). The differences between simulations and experiments (see Fig. 3) are attributed to noise sources that have not been simulated, such as non-linear frequency scan, intensity noise and the simplified seismic model. These differences are significantly reduced thanks to the GAN architecture, as shown in the results section of the paper.

V. Results

Initial results of the method's performance have been reported in [27]. The method was used there for discerning between

TABLE II
CLASSIFICATION ACCURACY FOR A 5 KM FIBER AND 3 CLASSES OVER ONE TRAINING SESSION (NOISE, FOOTSTEPS AND VEHICLES)

Training setup:	Accuracy	Confusion Matrix
Experimental dataset only	80.5%	**46%** 11% 43% 1% **96%** 3% 0.7% 0% **99.3%**
Simulation dataset only	40.3%	9.6% 21.5% **68.9%** 0% 18.5% **81.5%** 1.5% 5.9% **92.6%**
Simulation dataset only with refiner	64%	**66%** 24% 10% 1.5% **54%** 44.5% 2% 25% **73%**
Simulation dataset with refiner + fine-tune with experimental data	**83%**	**55%** 22% 23% 0% **94%** 6% 0% 0% **100%**

TABLE III
CLASSIFICATION ACCURACY FOR A 20 KM FIBER AND 3 CLASSES (NOISE, FOOTSTEPS AND VEHICLES)

Training setup:	Accuracy	Confusion Matrix
Experimental dataset only	42%	25.4% **42%** 32% 0 **99.5%** 0.5% 6.7% **91.5%** 1.8%
Simulation dataset only	35.4%	0% 0.04% **99.96%** 0% 9.8% **90.2%** 0% 3.6% **96.4%**
Simulation dataset only with refiner	50%	**49.6%** 15.6% 34.8% 8.9% 17.5% **73.6%** 4 % 12.9% **83.1%**
Simulation dataset with refiner + fine-tune with experimental data	80.2%	**79.5%** 5% 15.5% 7.1% **89.3%** 3.6% 2.2% 25.9% **71.9%**

footsteps at the vicinity of a 5 km fiber and ambient noise. It was shown that the proposed methodology enabled improvement of the detection accuracy from ∼52% (simulation only) to 94%. Adding a third class (vehicles) produced the results summarized in Table II. Despite the limited scale of the experimental dataset, the proposed approach led to a remarkable increase in classification accuracy. The confusion matrices at the right column of the table show cross-class classification between the three classes. The rows (from left to right) and columns (from top to bottom) in the matrices correspond to noise, footsteps and vehicles respectively.

Training the network on experimental data only classified correctly with high probability the footsteps and the vehicles (96% and 99.3% respectively) but the false alarm rate was very high (54%). Training on simulation data alone yielded poor performance. Once again, a marked increase in accuracy is observed when refined simulation data is used. Further improvement was obtained by fine-tuning this network with experimental data. Classification accuracy for footsteps achieves 94% and 100% for vehicles. The false alarm rate is reduced to 45%. While a much lower false alarm rate is desired, the current improvement shows the potential of the proposed method and its ability to produce valid train sets. Analyzing the performance of the algorithm's detection accuracy, i.e., only discerning between an event and noise, achieved a F1 score of 87.72% with experimental data only and increased to 89.85% using both the refined simulation and the experimental data.

A rough estimate for the robustness of the method was obtained by performing 6 sessions of training, based on refined-simulations and on refined-simulations + finetuning, on the 5 km datasets. The mean accuracies and their standard deviations were found to be 62.9% ± 1.7% and 83.1% ± 2.8% respectively.

The performance results for the 20 km sensing fiber experiment are summarized in Table III. The impact of the smaller experimental dataset and decreased SNR is evident. It can be seen that training on simulations alone is not effective and its accuracy is equivalent to a random classifier. Yet, the classification accuracy has improved from 42% to 80.2%, which is not very far from the 5 km case, thanks to the presented methodology. The F1 score for the detection performance of the algorithm started from 82.64% when trained on experimental data only and reached 87.23% using both the refined simulation and the experimental data.

In both the 5 km and the 20 km experiments, notice that a fair comparison was made between the different configurations of the network training. The training was based on two datasets - the costly experiment dataset and the "free" simulation dataset. Therefore, just setting their size to be equal is not a fair setup, especially because the experimental dataset contains true data and the simulation data is more simplistic. Thus, two cases should be focused on: (1) a comparison between training based on the simulation dataset only, with and without the refiner, and (2) a comparison between training based on the experimental dataset only and with the addition of the simulation data. In the first case, the clear improvement due to the refiner is visible when comparing the second and third rows of Tables II and III. In the second case, corresponding to the first and last rows of Tables II

and 3, the small and costly experimental dataset is used. The improvement between the first and last row of the results tables, is attributed to the mended initialization of the network originated from training with a refiner on the "free" and larger simulation dataset.

VI. Conclusions

Distributed fiber optic sensing technology is drawing tremendous interest due to its high sensitivity, high spatial resolution, immunity to electromagnetic interference and cost-effectiveness. As more and more systems are being purchased and deployed, the need for automatic and efficient data processing, detection and classification algorithms increases. While ANNs are ideal candidates for this task, the gathering of labeled data for their training is tedious and costly. In this paper, a deep learning approach for seismic data processing and its experimental testing is presented. Using GAN methodology, computer simulation data is refined and used to train ANN classifier. The GAN-trained network is shown to have significantly improved performance with respect to classifiers that are trained with simulation data only or experimental data only. Field experiments with 5 km and 20 km long sensing fibers are presented, with footsteps and vehicles excitations at their vicinity. Short time windows and narrow spatial segments make the method compatible with real time operation and localization abilities. Note that the proposed approach is compatible with real-time parallel computing as all fiber sections can be processed simultaneously.

Authors remark that no use of voting techniques is presented in this paper to emphasize the vanilla performances of the proposed methodology. Implementing such techniques could greatly improve accuracy performance.

To summarize, this study provides a proof-of-concept for the use of deep learning methodologies for classifying seismic data recorded by an optical fiber DAS system, and is adaptable to any fiber length and medium.

Acknowledgment

This research was supported by ERC-StG grant no. 757497 (SPADE) and Shlomo Shmeltzer Institute for Smart Transportation. The authors would like to thank NVIDIA for the GPU grant and the anonymous reviewers for their helpful and constructive comments that greatly contributed to improving this paper.

References

[1] A. Masoudi and T. P. Newson, "Contributed review: Distributed optical fibre dynamic strain sensing," *Rev. Sci. Instrum.*, vol. 87, no. 1, 2016, Art. no. 011501.

[2] L. Shiloh and A. Eyal, "Sinusoidal frequency scan OFDR with fast processing algorithm for distributed acoustic sensing," *Opt. Express*, vol. 25, no. 16, pp. 19205–19215, 2017.

[3] J. Pastor-Graells *et al.*, "SNR enhancement in high-resolution phase-sensitive OTDR systems using chirped pulse amplification concepts," *Opt. Lett.*, vol. 42, no. 9, 2017, Art. no. 1728.

[4] H. Xu, X. Zhang, Z. Zhang, and M. Li, "Study on pattern recognition method based on fiber optic perimeter system," *Proc. SPIE*, vol. 9679, 2015, Art. no. 96790Y.

[5] H. Zhu, C. Pan, and X. Sun, "Vibration waveform reproduction and location of OTDR based distributed optical-fiber vibration sensing system," *Proc. SPIE*, vol. 9062, 2014, Art. no. 906205.

[6] Q. Sun, H. Feng, X. Yan, and Z. Zeng, "Recognition of a phase-sensitivity OTDR sensing system based on morphologic feature extraction," *Sensors*, vol. 15, no. 7, pp. 15179–15197, 2015.

[7] A. Karpathy, G. Toderici, S. Shetty, T. Leung, R. Sukthankar, and L. Fei-Fei, "Large-scale video classification with convolutional neural networks," *Comput. Vis. Pattern Recognit.*, 2014, pp. 1725–1732.

[8] K. Simonyan and A. Zisserman, "Very deep convolutional networks for large-scale image recognition," in *Proc. 3rd IAPR Asian Conf. Pattern Recognit.*, 2015, pp. pp. 730–734.

[9] A. Krizhevsky, I. Sutskever, and G. E. Hinton, "Image net classification with deep convolutional neural networks," *Proc. Adv. Neural Inf. Process. Syst.*, 2012, pp. 1097–1105, 2012.

[10] Y. Lecun, K. Kavukcuoglu, and C. Farabet, "Convolutional networks and applications in vision," in *Proc. IEEE Int. Symp. Circuits Syst.*, 2010, pp. 253–256.

[11] S. K. Zhou, H. Greenspan, and D. Shen, *Deep Learning for Medical Image Analysis*. Amsterdam, The Netherlands: Elsevier, 2017.

[12] A. Van den Oord *et al.*, "WaveNet: A generative model for raw audio," in *Proc. 9th ISCA Speech Synthesis Workshop*, 2016, pp. 1–15.

[13] B. Karanov, M. Chagnon, F. Thouin, T. A. Eriksson, H. B¨ulow, and D. Lavery, "End-to-end deep learning of optical fiber communications," *J. Lightw. Technol.*, vol. 36, no. 20, pp. 4843–4855, Oct. 2018.

[14] S. Elmalem, R. Giryes, and E. Marom, "Learned phase coded aperture for the benefit of depth of field extension," *Opt. Express*, vol. 26, no. 12, pp. 5882–5891, 2018.

[15] A. Sinha, J. Lee, S. Li, and G. Barbastathis, "Lensless computational imaging through deep learning," *Optica*, vol. 4, no. 9, pp. 1117–1125, 2017.

[16] T. Baumeister, S. L. Brunton, and J. N. Kutz, "Deep learning and model predictive control for self-tuning mode-locked lasers," *J. Opt. Soc. Amer. B*, vol. 35, no. 3, pp. 617–626, 2018.

[17] Y. Rivenson, Z. Göröcs, H. Gunaydin, Y. Zhang, H. Wang, and A. Ozcan, "Deep learning microscopy," *Optica*, vol. 4, no. 11, pp. 1437–1443, 2017.

[18] W. Zhaoyong *et al.*, "Smart distributed acoustics/vibration sensing with dual path network," in *Proc. 26th Int. Conf. Opt. Fiber Sensors*, 2018, vol. 1, Paper WF105.

[19] H. Wu, C. Zhao, R. Liao, Y. Chang, and M. Tang, "Performance enhancement of ROTDR using deep convolutional neural networks," in *Proc. 26th Int. Conf. Opt. Fiber Sensors*, 2018, pp. 1–4.

[20] Q. Yan, Y. Yang, Z. Zhang, S. Jiang, Y. Xu, and C. Zhou, "Distributed vibration sensing system for oil and gas pipelines based on COTDR and BP neural network," in *Proc. 26th Int. Conf. Opt. Fiber Sensors*, 2018, Paper WF42.

[21] S. Liehr, L. A. Jäger, C. Karapanagiotis, S. Münzenberger, and S. Kowarik, "Real-time dynamic strain sensing in optical fibers using artificial neural networks," *Opt. Express*, vol. 27, no. 5, pp. 7405–7425, 2019.

[22] M. Aktas, T. Akgun, M. U. Demircin, and D. Buyukaydin, "Deep learning based multi-threat classification for phase-OTDR fiber optic distributed acoustic sensing applications," in *Proc. Commercial Sci. Sens. Imag.*, Apr. 2017, pp. 1–18.

[23] J. Tejedor *et al.*, "Towards prevention of pipeline integrity threats using a smart fiber optic surveillance system," *J. Lightw. Technol.*, vol. 34, no. 19, pp. 4445–4452, Oct. 2016.

[24] J. Tejedor *et al.*, "Real field deployment of a smart fiber-optic surveillance system for pipeline integrity threat detection: Architectural issues and blind field test results," *J. Lightw. Technol.*, vol. 36, no. 4, pp. 1052–1062, Feb. 2018.

[25] J. Tejedor *et al.*, "A Novel fiber optic based surveillance system for prevention of pipeline integrity threats," *Sensors*, vol. 17, no. 355, pp. 1–19, 2017.

[26] J. Tejedor, J. Macias-Guarasa, H. Martins, J. Pastor-Graells, P. Corredera, and S. Martin-Lopez, "Machine learning methods for pipeline surveillance systems based on distributed acoustic sensing: A review," *Appl. Sci.*, vol. 7, no. 8, 2017, Art. no. 841.

[27] L. Shiloh, A. Eyal, and R. Giryes, "Deep learning approach for processing fiber-optic das seismic data," in *Proc. 26th Int. Conf. Opt. Fiber Sensors*, 2018, Paper ThE22.

[28] I. J. Goodfellow *et al.*, "Generative adversarial networks," in *Proc. Adv. Neural Inf. Proc. Syst.*, 2014, pp. 2672–2680.

[29] A. Shrivastava, T. Pfister, O. Tuzel, J. Susskind, W. Wang, and R. Webb, "Learning from simulated and unsupervised images through adversarial training," in *Proc. IEEE Conf. Comput. Vision Pattern Recognit.*, 2016, pp. 2242–2251.

[30] L. A. Gatys, A. S. Ecker, and M. Bethge, "Image style transfer using convolutional neural networks," *Proc. IEEE Conf. Comput. Vis. Pattern Recognit.*, 2016, pp. 2414–2423.

[31] H. Sreter and R. Giryes, "Learned convolutional sparse coding," in *Proc. IEEE Int. Conf. Acoust., Speech, Signal Process.*, 2017, pp. 2191–2195.
[32] O. Litany, A. Bronstein, M. Bronstein, and A. Makadia, "Deformable shape completion with graph convolutional autoencoders," in *Proc. IEEE Conf. Comput. Vision Pattern Recognit.*, 2018, pp. 1886–1895.
[33] D. Arbel and A. Eyal, "Dynamic optical frequency domain reflectometry," *Opt. Express*, vol. 22, no. 8, pp. 8823–8830, Apr. 2014.
[34] C. Pan, H. Zhu, B. Yu, Z. Zhu, and X. Sun, "Distributed optical-fiber vibration sensing system based on differential detection of differential coherent-OTDR," in *Proc. IEEE Sensors*, 2012, pp. 26–28.
[35] H. Gabai and A. Eyal, "SNR characterization in distributed acoustic sensing," in *Proc. Int. Conf. Opt. Fibre Sensors*, vol. 9916, no. 3, 2016, Art. no. 99162W.
[36] M. Mirza and S. Osindero, "Conditional generative adversarial nets," in *NIPS Workshops: Deep Learn. Representation Learn.*, 2014, pp. 1–7.
[37] J. Deng, W. Dong, R. Socher, L. J. Li, K. Li, and F.-F. Li, "ImageNet: A large-scale hierarchical image database," in *Proc. IEEE Conf. Comput. Vis. Pattern Recognit.*, 2009, pp. 248–255.
[38] A. Odena, "Semi-supervised learning with context-conditional generative adversarial networks," in *ICML workshops: Data Efficient Mach. Learn.*, 2016, pp. 1–3.
[39] T. Salimans, I. Goodfellow, W. Zaremba, V. Cheung, A. Radford, and X. Chen, "Improved techniques for training GANs," in *Proc. Adv. Neural Inf. Process. Syst.*, 2016, pp. 1–10.
[40] T. Remez, O. Litany, R. Giryes, and A. M. Bronstein, "Class-aware fully-convolutional Gaussian and Poisson denoising," *IEEE Trans. Image Process.*, vol. 27, no. 11, pp. 5707–5722, Nov. 2018.
[41] E. Leviatan and A. Eyal, "High resolution DAS via sinusoidal frequency scan OFDR (SFS-OFDR)," *Opt. Express*, vol. 23, no. 26, pp. 33318–33334, 2015.
[42] H. Gabai and A. Eyal, "On the sensitivity of distributed acoustic sensing," *Opt. Lett.*, vol. 41, no. 24, pp. 5648–5651, 2016.